



HAL
open science

Facile Fabrication of Polymer Electrolytes via Lithium Salt-Accelerated Thiol-Michael Addition for Lithium-Ion Batteries

Ke Jiang, Jirong Wang, Cai Zuo, Shaoqiao Li, Sibao Li, Dan He, Haiyan Peng,
Xiaolin Xie, Rinaldo Poli, Zhigang Xue

► **To cite this version:**

Ke Jiang, Jirong Wang, Cai Zuo, Shaoqiao Li, Sibao Li, et al.. Facile Fabrication of Polymer Electrolytes via Lithium Salt-Accelerated Thiol-Michael Addition for Lithium-Ion Batteries. *Macromolecules*, 2020, 53 (17), pp.7450-7459. 10.1021/acs.macromol.0c01302. hal-02948181

HAL Id: hal-02948181

<https://hal.science/hal-02948181v1>

Submitted on 1 Mar 2021

HAL is a multi-disciplinary open access archive for the deposit and dissemination of scientific research documents, whether they are published or not. The documents may come from teaching and research institutions in France or abroad, or from public or private research centers.

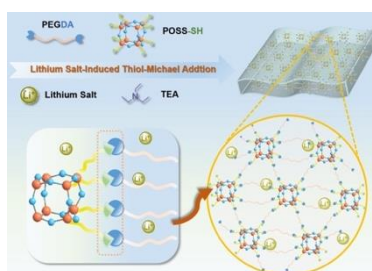
L'archive ouverte pluridisciplinaire **HAL**, est destinée au dépôt et à la diffusion de documents scientifiques de niveau recherche, publiés ou non, émanant des établissements d'enseignement et de recherche français ou étrangers, des laboratoires publics ou privés.

Facile Fabrication of Polymer Electrolytes via Lithium Salt-Accelerated Thiol-Michael Addition for Lithium-Ion Batteries

Ke Jiang,[†] Jirong Wang,[†] Cai Zuo,[†] Shaoqiao Li,[†] Sibao Li,[†] Dan He,[†] Haiyan Peng,[†] Xiaolin Xie,[†] Rinaldo Poli,^{*,‡} and Zhigang Xue^{*,†}

[†] Key Laboratory for Material Chemistry of Energy Conversion and Storage, Ministry of Education, School of Chemistry and Chemical Engineering, Huazhong University of Science and Technology, Wuhan 430074, P. R. China. [‡] CNRS, LCC (Laboratoire de Chimie de Coordination), Université de Toulouse, UPS, INPT, 205 Route de Narbonne, BP 44099, F-31077 Cedex 4, Toulouse, France.

For Table of Contents Use Only



ABSTRACT: Polymer electrolyte (PE) which possesses improved thermal and mechanical stability is believed by far one of the most promising electrolytes for meeting the safety and performance needs of advanced electrochemical devices. Here,

high-performance PEs are fabricated via facile thiol-Michael addition catalyzed by triethylamine in the presence of lithium salts. The lithium salt functions as both ion source and co-catalyst, significantly accelerating the thiol-Michael addition reaction. The PEs exhibits a superior thermal decomposition temperature up to 300 °C. Additionally, PEs from the thiol-decorated polyhedral oligomeric silsesquioxane display reversible electrochemical response and stable cycling performance. Our finding based on a self-catalyzed strategy provides a promising direction for rapidly fabricating PEs that meet electrochemical requirements for practical solid polymer batteries.

INTRODUCTION

The increasing demand for electric vehicles and efficient energy storage devices promotes the development of rechargeable batteries with high energy density and long cycle life.¹⁻⁶ However, lithium-ion batteries (LIBs) with liquid organic electrolytes have brought security and reliability concerns owing to inherent limitations such as high volatility, leaks, and explosions.^{7,8} It is thus expected that replacing conventional liquid organic electrolytes with polymer electrolytes (PEs) can improve the Li-based battery safety, performance, and machinability.⁹⁻¹² The poly(ethylene oxide) (PEO) has been most widely studied for PE systems because of its high dielectric constant and ability to form complex with lithium salts.^{13,14} Nevertheless, lithium-salt doped PEO exhibits low ionic conductivity at room temperature originating from its semi-crystalline nature, which hampers the transport of lithium ions through the polymer chain segments.¹⁵

Building a cross-linked framework¹⁶⁻²¹ or loading inorganic components into the polymer matrices²²⁻²⁸ can efficiently improve ionic conductivity by inhibiting the crystallization and simultaneously enhance the mechanical properties of the PEs.

The thiol-ene reaction can generally proceed via either radical-mediated anti-Markovnikov addition or base- or nucleophile-catalyzed thiol-Michael addition.²⁹⁻³¹ Owing to the rapid reaction kinetics, high efficiency, chemo-selectivity, and benign reaction conditions, the thiol-ene reaction has become a particularly useful tool in polymer chemistry and materials science,³²⁻³⁶ including polymer network construction, surface functionalization and dendrimer synthesis. For instance, Saito *et al.*³⁶ synthesized poly(dimethylsiloxane)-poly(ethylene glycol) methyl ether acrylate (PDMS-PEGMEA)-based co-polymer membranes via UV initiated one-pot thiol-ene reaction to fabricate elastic polymer materials used for gas separation application. Fang *et al.*³⁷ used thiol-ene reaction to prepare two flexible and colorless phosphorous-sulfide polymer films based on a phosphorus-containing derivative of aromatic aldehyde (4-hydroxybenzaldehyde). Grewal *et al.*³⁸ and Suk *et al.*³⁹ reported polymer electrolytes based on a crosslinked network formed via thiol-ene reaction using a thermal initiator. However, it is difficult to obtain an ideal 1:1 stoichiometric reactivity through conventional free radical-mediated addition, which means the simultaneous existence of thiol-ene and ene-ene reaction will most probably pose difficulties for the acquisition of well-defined polymer structure.⁴⁰ To tackle this problem, several approaches are proposed by researchers. Bowman and co-workers⁴¹⁻⁴³ synthesized visible-light-sensitive photo-base generators applied in thiol-Michael addition reactions, which

allows a stoichiometric reaction of both thiol and vinyl functional groups and enables homogeneous network formation. Photopolymerization, as well as the introduction of allyl groups, has been an effective method to develop a controlled network through precise design of the polymer structure, but the complicated synthesis and severe operation condition limit the practical application. Thus, a convenient fabrication process is necessary to form PEs with improved ionic conductivity, high thermal stability, and excellent cycling performance, which can be achieved by using thiol-Michael addition. Thiol-Michael addition is modular in nature, highly efficient, and exhibits stoichiometric reactivity of 1:1, hence classified as a “click” reaction. By the adjunction of minimal dosage of catalysts (base or nucleophilic reagent) under ambient temperature, it can occur without any exposure to heat or light. In recent years, the thiol-Michael addition has been employed in a large extent of applications, such as small molecule synthesis, surface functionalization, bioconjugation, tissue engineering, dendrimer synthesis, and polymer network synthesis.³²

The self-catalyzed strategy is an attractive method to fabricate PEs via a simple preparation routine with the lithium salts employed as ion sources on one hand and as catalysts on the other hand. In 2001, Tsutsumi and co-workers⁴⁴ reported that various lithium salts could initiate the cationic ring-opening polymerization (ROP) of bis-oxetanes, indicating the potential of self-catalyzed strategy in polymer electrolyte field. Cui *et al.*⁴⁵ reported a crosslinked PE by a self-catalyzed strategy and in-situ technology via a facile cationic polymerization initiated by lithium salts. Recently, Li *et al.*⁴⁶ used LiPF₆ to induce the cationic polymerization of the ether-based 1,3-dioxolane and 1,2-

dimethoxyethane liquid electrolyte and fabricated quasi-solid gel PEs. Archer *et al.*⁴⁷ reported cationic aluminum species-initiated ROP of 1,3-dioxolane inside an electrochemical cell to produce PEs. The self-catalyzed strategy offers incomparable advantages including facile preparation procedure, efficiency, high production and low costs. Yet, the uncontrollability of chain-growth polymerization is hardly satisfactory if the formation of a well-defined polymer electrolyte network is desired. More importantly, compared with electrolytes formed via the self-catalyzed strategy, which are neat polymer matrices, preparing composite polymer electrolytes with inorganic nanofillers introduced is an effective strategy to enhance the ionic conductivity and cycling stability of LIBs. Several studies on organic-inorganic hybrid polymer electrolytes have certificated the mechanism of ionic conductivity enhancement, the interactions between polymer matrix and inorganic fillers at the interface.⁴⁸ First, due to chemical or/and physical interactions, polymer segments can be attracted by the surface sites of ceramic fillers, providing amorphous-rich areas as Li⁺ transport channels near surface region of inorganic fillers. Second, there are intense interaction between anionic groups of lithium salts and chemical groups of ceramic fillers, promoting the lithium salts dissociation and leading to the increase of free Li⁺ concentration at the interface. Third, the interaction between polymer chains and inorganic fillers could influence the local conformation of segments in polymer, which probably provides Li⁺-conductive substructures for polymer matrix. Moreover, compared with neat polymer matrix, the cycle stability of composite polymer electrolytes could be improved because the mechanical strength inorganic fillers

provided is helpful to prevent the growth of lithium dendrites.⁴⁹ Cui *et al.*⁵⁰ reported a composite polymer electrolyte with vertically aligned ceramic-polymer interfaces, achieving high interfacial ionic conductivity and long cycle life when compared to the PE without nanofillers.

Herein, we applied the thiol-Michael addition as a platform to fabricate cross-linked electrolytes with well-defined network by employing a selection of multifunctional thiols, poly(ethylene glycol) diacrylate (PEGDA, $M_n = 200, 400, \text{ or } 600$) with triethylamine (TEA) as a catalyst in the presence of lithium salts (**Figure 1**). Studies on the polymerization kinetics denote that lithium salts (lithium perchlorate, lithium bis(trifluoromethanesulfonyl)imide and lithium trifluoromethanesulfonate) are capable of significantly accelerating the base-catalyzed thiol-Michael addition, which enables them to act as ion sources as well as co-catalysts in the polymerization. Moreover, some other alkali metal salts including sodium perchlorate and potassium perchlorate have also shown the same effect as the lithium salts. The novel self-catalyzed strategy for the base-catalyzed one-pot thiol-Michael addition reaction under ambient temperature described in the present work provides a facile fabricating procedure of PEs. Furthermore, we introduce the thiol-decorated polyhedral oligomeric silsesquioxane (POSS-SH, **Figure S1**, Supporting Information) into electrolyte networks, which plays an important role in promoting the thermal performance and decreasing the crystallinity of PEs because of the intramolecular organic-inorganic hybrid structure. Moreover, the ideal 1:1 stoichiometric reactivity of thiol group and acrylate group will be conducive to the uniform dispersion of POSS and effectively

avoid agglomeration of nano-particles, which can lead to negative impact on polymer electrolytes, including growth of lithium dendrite, poor interfacial contact between electrode and polymer electrolytes, and increase of interfacial impedance. As a result of the cross-linked structure and presence of the inorganic component, the ionic conductivity and mechanical property of PEs are also enhanced. The constructed LIBs on the basis of these PEs as separators, lithium iron phosphate (LFP) as cathode and lithium metal as anode show impressive electrochemical performances including a stabilized plating/stripping process and promising cycling property.

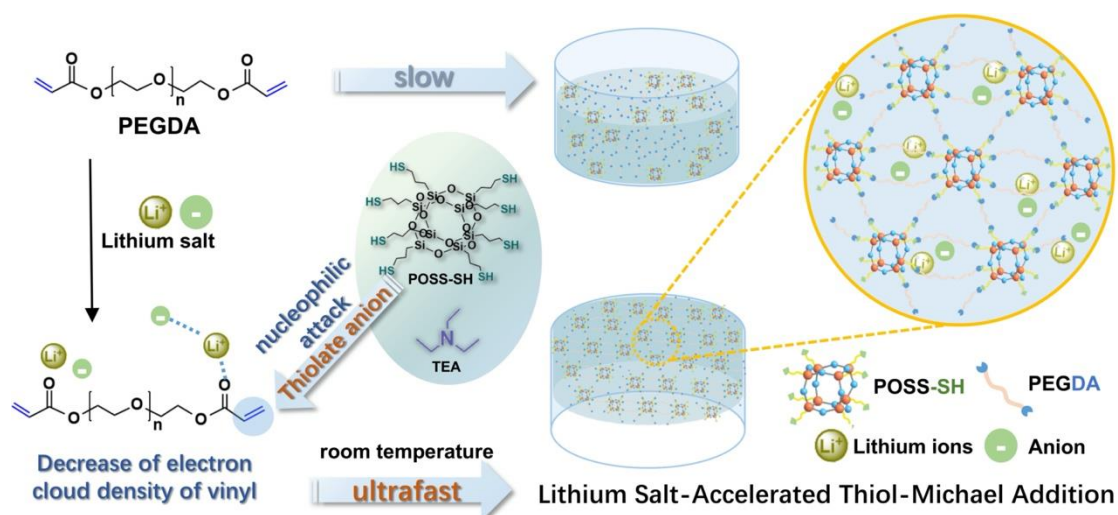


Figure 1. Schematic illustration of the formation of PEs using PEGDA₆₀₀ and POSS-SH catalyzed by TEA in the presence of lithium salts.

EXPERIMENTAL SECTION

Materials. (3-Mercaptopropyl)trimethoxysilane (KH-590, 95%, Aladdin), trimethylolpropane tris(3-mercaptopropionate) (TMPTMP, 95%, Sigma-Aldrich), pentaerythritol tetra(3-mercaptopropionate) (PETMP, 90%, Aladdin), 1-hexanethiol (HT, 96%, Aladdin), and poly (ethylene glycol) diacrylate (PEGDA, $M_n = 200, 400,$ or $600,$ Aladdin) were used as received. Triethylamine (TEA) and tetrahydrofuran (THF)

were dried with calcium hydride and distilled under reduced pressure before use. Lithium perchlorate (LiClO_4 , 99.9%, Aladdin), lithium bis(trifluoromethanesulfonyl)imide (LiTFSI , 99%, Aladdin), lithium trifluoromethanesulfonate (LiCF_3SO_3 , 98%, Aladdin), sodium perchlorate (NaClO_4 , 99.5%, Aladdin), and potassium perchlorate (KClO_4 , 99%, Aladdin) were dried under vacuum and stored in argon-filled glovebox before use. Other chemicals, including hydrochloric acid (HCl), methanol, dichloromethane (CH_2Cl_2), lithium iron phosphate (LiFePO_4 , LFP), acetylene black (AB), poly-(vinylidene fluoride) (PVDF), and *N*-methyl-2-pyrrolidone (NMP) were purchased locally.

Synthesis and Characterization of POSS-SH. 15 mL KH-590 and 30 mL HCl were dissolved in 350 mL methanol. Then the mixture was stirred vigorously under reflux with oil bath at 90 °C for 24 h. The reaction product was separated by centrifugation to obtain white precipitate and washed with methanol to give the crude product. The crude product was poured into H_2O and extracted with CH_2Cl_2 . The organic layers were washed with H_2O for several times, and then dried with Na_2SO_4 . Finally, the product was evaporated on a rotary evaporator and dried under vacuum at 60 °C for 24 h. The ^1H NMR spectra of prepared POSS-SH is listed in **Figure S1**. The characteristic peaks at 0.77, 1.71 and 2.57 ppm represent protons of three different methylene respectively. Meanwhile, the characteristic peak at 1.38 ppm is assigned to the proton of thiol group. And the mass spectroscopy of POSS-SH is shown in **Figure S2**, which suggests that the polyhedral oligomeric silsesquioxane conform to the m/z of T_8 conformation plus Cl^- .

Fabrication of Polymer Electrolytes. PEs were prepared through a solution casting technique and thiol-Michael addition with TEA as the catalyst and LiClO₄ as the co-catalyst. PEGDA ($M_n = 600$, 2.5 mmol), POSS-SH (thiol/vinyl = 1:1, 0.625 mmol) and LiClO₄ (EO/Li⁺ = 16:1, 1.68 mmol) were dissolved in THF (10 mL) in a round flask and stirred for 3 h at room temperature. TEA (1 wt%, 30 μ L) was then dripped into the flask. The solution was stirred vigorously for 10 s and then cast in a polytetrafluoroethylene (PTFE) mold. The reaction occurred under air atmosphere and at room temperature, and the membranes were dried under vacuum at 60 °C for 24 h to remove THF. The PEs were obtained and stored in a glove box.

Characterization of Polymer Electrolytes. NMR spectra was measured with CDCl₃ as solvent by a Bruker AV400 NMR spectrometer. FT-IR spectroscopy was performed on an FT interferometer (Equinox 55, Bruker, Germany) over the range of 4000-400 cm⁻¹. The homogeneity of PEs was estimated by scanning electron microscopy (SEM) and energy dispersive X-ray (EDX) mapping (Nova NanoSEM450, FEI, Netherlands).

Thermogravimetric analysis (TGA, 4000 PerkinElmer, USA) under N₂ with a heating rate of 10 °C min⁻¹ from 30 to 800 °C and differential scanning calorimetry (DSC, Q2000, TA, USA) under N₂ atmosphere with a ramp rate of 10 °C min⁻¹ from -90 to 90 °C were employed to characterize the thermal performance of the PEs.

The ionic conductivity of PEs was determined using an electrochemical test system (Autolab PGSTAR302N, Netherlands) via electrochemical impedance (EIS) analysis. The data were collected with temperatures ranging from 30 °C to 110 °C at 10 °C intervals over a frequency range from 1 MHz to 100 Hz. The PEs membranes were

sandwiched between two stainless steel (SS) electrodes. The ionic conductivity was calculated via the equation $\sigma = L/(SR_b)$, where L is the thickness of the polymer electrolyte membrane, S is the contact area between SS electrode and electrolyte, and R_b is the bulk electrolyte resistance.

The electrochemical stability of PEs was estimated via linear sweep voltammograms (LSV) using the Li | PEs | SS cells at a scan rate of 0.1 mV s^{-1} over the range of 0-6 V at $60 \text{ }^\circ\text{C}$. The Li | PEs | Li cells were applied to evaluate the lithium ion transference number (t_{Li^+}) by the equation $t_{\text{Li}^+} = I_s(\Delta V - I_0 R_0)/I_0(\Delta V - I_s R_s)$. The cell was polarized at 10 mV (ΔV) to determine the currents including the initial (I_0) and the steady state (I_s) until the current was steady. Interfacial resistances were obtained before (R_0) and after (R_s) the polarization.

The lithium electrodeposition was employed to investigate the interfacial stability between PEs and lithium metal using Li | Li CR2032 coin cells. The plating/stripping efficiency of Li metal was tested with a current density of 0.05 mA cm^{-2} at $60 \text{ }^\circ\text{C}$.

LiFePO₄, carbon black, and PVDF were mixed with a weight ratio of 8:1:1. The slurry was coated on aluminum foil and dried under vacuum at $85 \text{ }^\circ\text{C}$ for 24 h. The CR2032 coin cells were assembled with PEs, Li anode and LFP cathode in an argon-filled glovebox. The charge-discharge and cycling performances were tested at $60 \text{ }^\circ\text{C}$ under the potential window of 2.5-4.2 V by a battery testing system (LANHE CT2001A).

DFT Calculations. The computational work was carried out using the Gaussian09 suite of programs.⁵¹ Gas-phase geometry optimizations were performed without any

symmetry constraint using the B3LYP functional and the 6-31G(d,p) basis functions for all atoms. Dispersion interactions were taken into account by Grimme's D3 empirical method during the geometry optimizations (B3LYP-D3).⁵² All final geometries were characterized as stationary points by verifying that all second derivatives of the energy were positive. Thermochemical corrections were obtained at 298.15 K on the basis of frequency calculations, using the standard approximations (ideal gas, rigid rotor and harmonic oscillator). A solvation correction was carried out on the gas-phase optimized molecules by fixed-geometry calculations in the presence of a polarizable continuum with the Gaussian09 library values for the permittivity of chloroform ($\epsilon = 4.7113$) or THF ($\epsilon = 7.4257$). A further correction of 1.95 kcal mol⁻¹ was applied to bring the G values from the gas phase (1 atm) to the solution (1 mol L⁻¹) standard state.⁵³ The NMR spectra in chloroform solution were calculated by the Gaussian09 package using the standard Gauge-Independent Atomic Orbital (GIAO) method.⁵⁴

RESULT AND DISCUSSION

Physical Structure and Characterizations. **Figure S3** presents typical images of the ultrafast formation of a cross-linking network by PEGDA₆₀₀ and pentaerythritol tetra(3-mercaptopropionate) (PETMP) via TEA-catalyzed thiol-Michael addition in the presence of several types of alkali metal salts within 30 seconds at room temperature. Continuous observation of the reaction catalyzed only by TEA shows that no cross-linked network forms after 3 hours. Images of the corresponding reaction of PEGDA₆₀₀ and POSS-SH are depicted in **Figure 2a**, where 5 mL of THF was added in each experiment to guarantee full dissolution of POSS-SH. The reaction is slower than that

with PETMP, but the gelification was achieved within 10 min in the presence of LiClO_4 and LiTFSI , whereas the solution containing TEA only changed from the liquid to the solid state after 60 h. It is obvious that this self-catalyzed strategy via thiol-Michael addition allows the rapid construction of PEs. The Fourier transform infrared (FT-IR) analysis shows that the characteristic peaks of the POSS-SH thiol groups at 2550 cm^{-1} and of the PEGDA₆₀₀ vinyl moiety at 1630 cm^{-1} fade away after the thiol-Michael addition (**Figure S4**), confirming that the PEGDA₆₀₀ and multifunctional thiols monomers have reacted completely. The uniform distribution of carbon, oxygen, silicon, and sulfur elements, shown by the energy dispersive X-ray (EDX) analysis of cross-section (**Figure 2b**), suggests that no significant inorganic nanoparticles aggregation occurs (the original SEM image is shown in **Figure S5**). This good dispersibility of inorganic fillers is beneficial for the improvement of the mechanical properties.⁵⁵

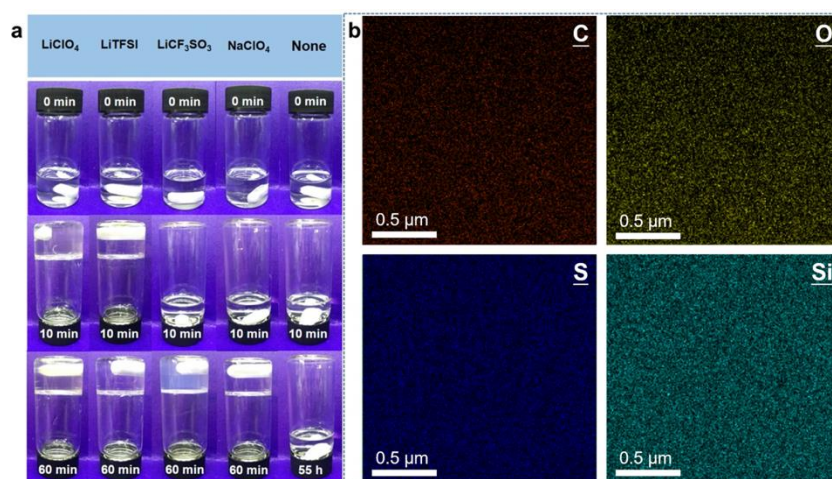


Figure 2. (a) Digital images of PEGDA₆₀₀ and POSS-SH mixed with alkali metal salts. (b) EDX maps of PEGDA₆₀₀-S-POSS.

The real-time FT-IR spectroscopy was also employed to reveal the reaction kinetics of the TEA-catalyzed thiol-Michael addition using PEGDA₂₀₀ and 1-hexanethiol (HT) as model substrates by monitoring the disappearance of acrylate and

thiol peaks (**Figure S6**). In the absence of LiClO_4 , this addition reaction proceeded slowly, reaching only about 3% conversion of both vinyl and thiol groups in 30 min, whereas the reaction proceeds to nearly full conversion in 30 min in the presence of the salt (**Figures 3a** and **3b**). The kinetics of the reaction does not strongly depend on the $\text{PEGDA}_{200}:\text{LiClO}_4$ ratio (**Figure S7**). **Figure S8** shows that no significant conversion of the thiol and vinyl groups for the mixture of PEGDA_{200} and HT takes place after 1 h in the absence of TEA, even if LiClO_4 is present ($\text{PEGDA}_{200} : \text{LiClO}_4 = 20:1$). This result clearly establishes that both TEA and LiClO_4 are essential to accelerate the reaction. The time-conversion curves for the reactions carried out in the presence of a few other alkali metal salts, including LiTFSI , LiCF_3SO_3 , NaClO_4 , and KClO_4 (**Figures 3a** and **3b**) illustrate that they also function as co-catalysts, especially LiTFSI , LiCF_3SO_3 and NaClO_4 .

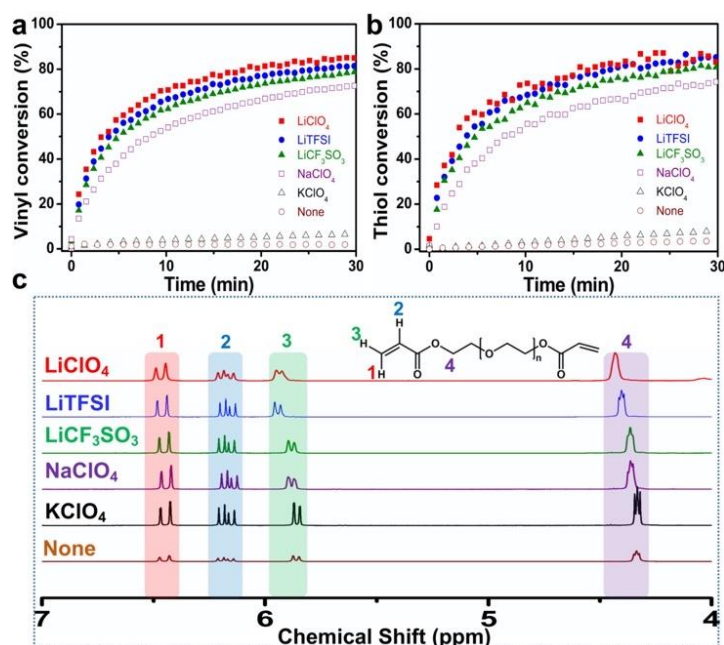


Figure 3. Conversion against time of vinyl (a) and thiol (b) group for the TEA-catalyzed thiol-Michael addition of PEGDA_{200} and 1-hexanethiol (HT). $[\text{HT}] : [\text{PEGDA}_{200}] : [\text{TEA}] = 2:1:0.043$ (thiol : vinyl = 1:1) in the presence of different alkali metal salts ($[\text{PEGDA}_{200}] : [\text{salts}] = 20:1$). (c) ^1H NMR spectra (CDCl_3) of PEGDA_{600} with different alkali metal salts ($[\text{PEGDA}_{600}] : [\text{salts}] = 1:2$).

DFT Calculations and Mechanistic Aspects. It is known that the double bond conjugation in acrylate substrates renders the vinyl group electron deficient and therefore suitable for the thiol-Michael addition because the nucleophilic attack by a thiolate anion is accelerated. In addition, stronger electron withdrawing groups should lead to greater electron deficiency and therefore to higher reactivity. We can imagine that coordination of Li^+ to the oxygen from carbonyl moiety of the acrylate group decreases the vinyl group electron density, thus leading to a faster reaction. To evaluate this hypothesis, we tested the interaction between different salts and the acrylate group by ^1H NMR spectroscopy in CDCl_3 (**Figure 3c**), where all salts were fully dissolved. In comparison with pure PEGDA_{600} , the methylene proton signals of the $\text{PEGDA}_{600}/\text{LiClO}_4$ mixture shift to lower field, suggesting a decreased electron density for the vinyl group. The resonance shifts are greater for greater LiClO_4 to PEGDA_{600} ratios (**Figure S9a**). The resonance shift is also evident for the other lithium salts, particularly for LiTFSI where the larger anion may favor a stronger salt dissociation, and also for NaClO_4 , whereas KClO_4 has a negligible effect. The position of methylene proton signals also remains essentially unchanged when PEGDA_{600} is mixed with TEA only (**Figure S9c**), indicating that TEA does not have the same effect of decreasing the vinyl electron density.

The above hypotheses were also supported by density-functional theory (DFT) calculations, which provided, in addition, an insight into the reaction mechanism. The effect of the salt interaction with the acrylate function was probed by performing calculations on adducts of methyl acrylate, as a model substrate, with MtClO_4 ($\text{Mt} = \text{Li}$,

Na, K) in the presence of a polarizable continuum to model the chloroform solvent. Full details are provided in the Supporting Information. Since chloroform has poor coordinating properties, the salt was introduced in the calculation without explicit solvent molecules. In addition to showing a favorable interaction in the order $\text{Li} > \text{Na} > \text{K}$ ($\Delta G_{\text{D3,298K,CHCl}_3} = -19.1, -15.7$ and $-10.8 \text{ kcal mol}^{-1}$, respectively), the calculations predict that the $\text{O} \cdots \text{Mt}$ interaction lengthens the $\text{O}=\text{C}$ bond and slightly shortens the $(\text{O})\text{C}-\text{C}$ bond, whereas the vinyl $\text{C}=\text{C}$ bond remains practically unaltered, while increasing the Mulliken charge on all three vinyl H atoms (details in **Table S1**). These effects are again decreasing in the order $\text{Li} > \text{Na} > \text{K}$. Finally, the calculations predict a downfield shift of the ^1H NMR resonance for all three vinyl H atoms, relative to free MA, in agreement with the experimental trend (**Table S1**).

The DFT calculations cannot pinpoint the role of the cation on the activation barrier for the thiol-Michael addition, because the effects of the explicit coordination of solvent molecules (THF) to the alkali cation and of ion pairing cannot be easily modelled computationally. The calculations have provided, however, useful information on the reaction mechanism, which allow the suggestion of the possible role of the cation. The reaction pathway was probed using again MA as a model substrate and MeSH as a computational model for the thiol reagent. A polarizable continuum model with the permittivity of THF, which was the reaction solvent, was used in this case. Michael additions are known to proceed by nucleophilic attack at the C_β and yield an enolate intermediate, followed by quenching by protonation, see **Scheme S1a**. In the absence of base, the nucleophile (MeSH) is too weak and cannot yield the enolate

intermediate. Rather, the assistance by a second MeSH molecule is necessary and the reaction proceeds by a concerted mechanism, with the simultaneous delivery of the thiolate from one MeSH molecule to C_β and the proton from the second MeSH molecule to C_α, with a high barrier ($\Delta G_{298, \text{THF, 1M}} = 36.1 \text{ kcal mol}^{-1}$). The mechanism is presented in **Scheme S1b** and the energy profile is shown in **Figure S10**.

The energy barrier for the thiol addition is greatly reduced upon thiol deprotonation. The putative free enolate MeSCH₂CH=C(OMe)O⁻ product resulting from addition of the thiolate anion (MeS⁻) could not be obtained as a local energy minimum, converging instead to a loose MA···SMe⁻ adduct with a S···C_β contact of 2.888 Å, which is much longer than in the final MeS-CH₂CH₂COOMe product (1.834 Å). This adduct is destabilized relative to the sum of the reagents by 3.0 kcal mol⁻¹. Addition of the proton-delivering thiol molecule to the system further raises the free energy, although only slightly (3.2 kcal mol⁻¹) and produces a van der Waals adduct between MA and the homoconjugate thiol-thiolate pair, [MeSH···SMe]⁻, without any MeSH···MA interaction. The nucleophilic attack is very facile, with a free energy barrier of only 6.9 kcal mol⁻¹ relative to the sum of all reagents, to yield an intermediate, [MeSCH₂CH(COOMe)]⁻···HSMe, which is located at essentially the same free energy as the transition state. In this intermediate, a significant negative charge is localized on the C_α atom, which is slightly pyramidalized, and the proton delivering MeSH molecule establishes a C_α···H-SMe interaction. Then, proton transfer to this intermediate is essentially barrierless, as shown by a relaxed scan (the transition state could not be located). Hence, the anionic addition pathway indeed occurs in a stepwise manner, but

the intermediate is better described as a carbanion than as an enolate, see **Scheme S1c**. However, we must keep into account that the generation of the thiolate anion is thermodynamically unfavorable, because the conjugate acid of NEt_3 , namely the ammonium cation Et_3NH^+ , is a stronger acid than the thiol. Indeed, a ^1H investigation of the reaction between 1-hexanethiol and NEt_3 gave no evidence of proton transfer (**Figure S11**). The DFT calculations indicate that NEt_3 and the model thiol MeSH produce an H-bonded $\text{MeS-H}\cdots\text{NEt}_3$ adduct, located $0.4 \text{ kcal mol}^{-1}$ higher in free energy, and the subsequent proton transfer is highly endoergic ($\Delta G_{298,\text{THF},1\text{M}} = 25.3 \text{ kcal mol}^{-1}$ for the sum of the separated ions, NHet_3^+ and MeS^-). The $\text{NHet}_3^+\cdots\text{SMe}$ ion pair did not yield a stable minimum, reverting back to the H-bonded adduct during the optimization. Hence, the overall barrier for the NEt_3 -catalyzed thiol Michael addition to acrylate is only slightly decreased (to $32.2 \text{ kcal mol}^{-1}$, see **Figure S10**) when also considering the cost of the thiol deprotonation.

The experimental results clearly demonstrate that the presence of an alkali metal cation reduces the reaction energy span. However, the computational quantification of this effect is not straightforward because, as stated above, solvent coordination and ion pairing/free ion equilibria are not trivial to model. Optimization attempts of the intermediate enolate, $\text{MeS-CH}_2\text{CH}=\text{C}(\text{OMe})(\text{O}^-\cdots^+\text{Cat})$ converged in all cases to the sum of the reagents ($\text{MA}\cdots\text{Cat}(\text{SMe})$), whether a naked metal ion (Mt^+) or a more realistic model of the solvated cation ($[\text{Mt}(\text{Me}_2\text{O})_3]^+$, with the Me_2O ligands used as the computational model for THF), was used as cation. A stable local minimum could only be obtained for the *anti*-conformation of the $\text{C}_\alpha\text{-C}_\beta$ bond, separating the MeS group

from the cation. The $\text{MeSCH}_2\text{CH}=\text{C}(\text{OMe})[\text{OMt}(\text{Me}_2\text{O})_3]$ enolates were weakly destabilized relative to the sum of the MA and $\text{MeS}[\text{Mt}(\text{Me}_2\text{O})_3]$ reagents by about the same amount for the three cations (Li, 2.0; Na, 1.7; K, 2.1 kcal mol⁻¹). Local minima could be located, however, after adding a MeSH molecule to the systems with the naked cations, which also corresponds to the addition of Mt^+ to the intermediate of the anionic pathway presented above. The optimized geometries of all these intermediates are comparatively shown in **Figure S12**. All of them show a relatively strong $\text{Mt}^+\cdots\text{O}$ interaction, but also feature $\text{Mt}^+\cdots\text{S}$ interactions involving both the free MeSH molecules and the MeS group that is already incorporated in the enolate intermediate. In addition, the Na and K systems also show an additional $\text{S-H}\cdots\text{C}_\alpha$ hydrogen bond, like in the cation-free intermediate.

The reaction pathway for the thiolate Michael addition in the presence of Mt^+ could also be investigated starting from MA, $\text{Mt}^+(\text{SMe}^-)$ and MeSH and the results are shown in **Figures S13-S15**. In these cases, the transition states for the final proton transfer step from MeSH to the C_α atom could be optimized, whereas those of the first step (MeS⁻ addition to the C_β atom) could not. All these reactions have relatively low barriers, at about the same energy relative to the sum of the three separate fragments. The initial addition of $\text{Mt}^+(\text{SMe}^-)$ to MA is exoergic in the order $\text{Li} > \text{Na} > \text{K}$. Placing these pathways on the same scale relative to MA (plus MeSH, NEt_3 and $\text{Mt}^+\text{ClO}_4^-$) requires however assessment of the ion metathesis between $\text{Mt}^+\text{ClO}_4^-$ and $\text{Et}_3\text{NH}^+\text{MeS}^-$. This was probed using again the naked cation, yielding the results shown in **Figures S13-S15**. The most interesting result is that the ion metathesis is quite favorable, thus

the proton transfer from MeSH to NEt_3 in the presence of $\text{Mt}^+\text{ClO}_4^-$ (leading to $\text{MtSMe} + \text{Et}_3\text{NH}^+\text{ClO}_4^-$) is less energetically costly than in the absence of salt. These results should not be considered as quantitatively reliable, because of the unrealistic model with neglect of solvent coordination to the alkali cation. Another drastic approximation is the neglect of the ion pair dissociation to the free ions. This dissociation likely becomes more favorable for the larger cations ($\text{K} > \text{Na} > \text{Li}$), thus the energetic cost of the initial proton transfer, which also reflects onto the energy of the rate-determining transition state, is probably greater than what is shown in **Figures S13-S15**, approaching the energetic cost calculated in the absence of salt in **Figure S10**. In spite of all these approximations, the study qualitatively suggests that the reaction is accelerated, because the energy needed to bring together the anionic nucleophile and the substrate is lowered, which is owing to the more favorable ion pairing in the $\text{Et}_3\text{NH}^+\text{ClO}_4^-$ and Mt^+SMe^- salts than in the metathesized pair ($\text{Mt}^+\text{ClO}_4^-$ and $\text{Et}_3\text{NH}^+\text{SMe}^-$).

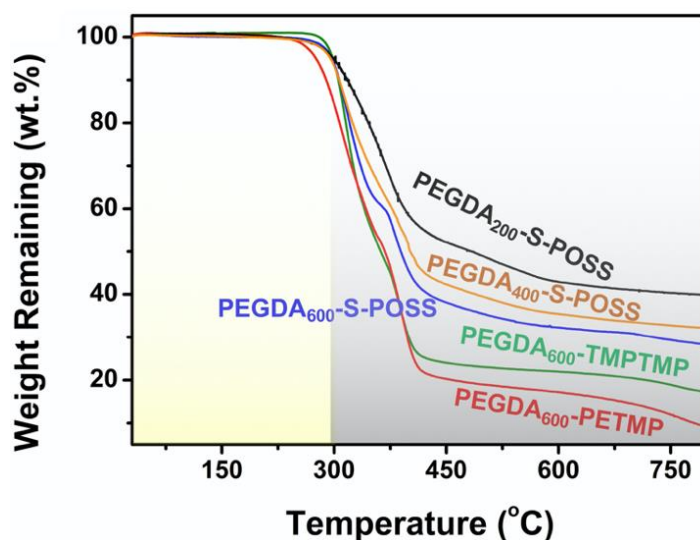


Figure 4. Thermogravimetric analysis (TGA) curves of PEs.

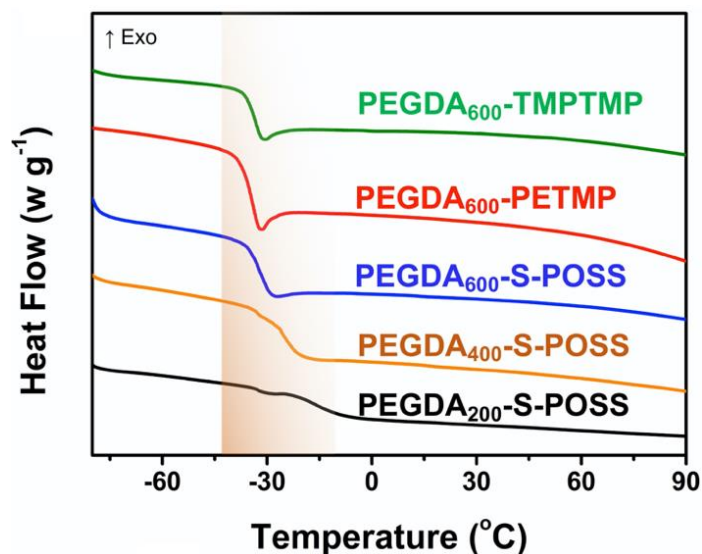


Figure 5. Different scanning calorimetry (DSC) analysis of PEs.

Thermal and Mechanical Properties. Thermal stability is one of the most critical criteria to assess the potential application of PEs in LIBs. As shown in **Figure 4**, the PEs with the cross-linking structure possess a high decomposition temperature (~ 300 °C), which is advantageous to the safety performance of LIBs. The glass transition temperature (T_g) is also a crucial performance standard to evaluate the ionic conductivity of the PEs. In particular, owing to the cation-oxygen complexation in the PEO/Li-salt mixture, the transient physical cross-linking between different PEO segments leads to slower chain relaxation, higher T_g , which is to the disadvantage of improvement of ionic conductivity.⁵⁶ T_g decreases with an increase of the PEGDA molecular weight, as shown by the different scanning calorimetry (DSC) analyses (**Figure 5** and **Table S3**), because longer PEGDA chains are capable of promoting the molecular relaxation of the PEs. Besides, the T_g values of PEGDA₆₀₀-TMPTMP (TMPTMP refers to trimethylolpropane tris(3-mercaptopropionate)) and PEGDA₆₀₀-PETMP are also lower. The toughness of PEs is important to restrain growth of lithium

dendrite and prevent from penetration, which can be characterized by tensile test. In general, tensile stress is utilized to assess intrinsic resistance for fracture of polymer materials.⁵⁷ Thus, the tensile stress is available to estimate the resistance for fracture when lithium dendrites penetrate the PEs.⁵⁸ The tensile stress of the PEGDA₆₀₀-S-POSS PE reaches 310 kPa (**Figure S16**), demonstrating good mechanical strength and suggesting that this PE can meet the requirements for their practical applications in LIBs.

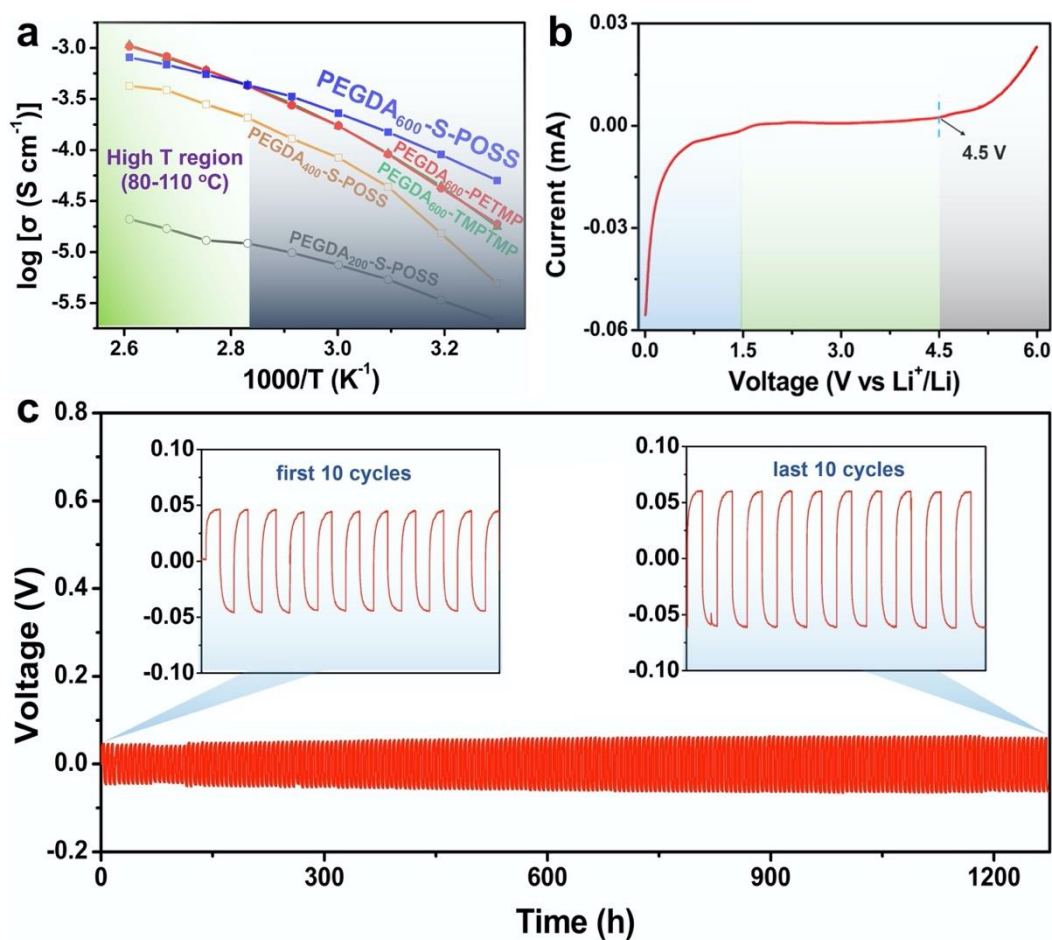


Figure 6. (a) Temperature dependence of the ionic conductivity of PEs. (b) LSV curve of PEGDA₆₀₀-S-POSS at 60 °C. (c) Galvanostatic cycling performance of Li | PEGDA₆₀₀-S-POSS | Li symmetric battery measured at 60 °C with current density of 0.05 mA cm⁻² with capacity of 0.15 mAh cm⁻². Insets: enlarged profiles of the first 10 cycles and last 10 cycles.

Electrochemical Performances. Generally, only the amorphous fraction of PEO is beneficial to ionic conduction because cation transport is coupled with the PEO mobility.⁵⁹ The ionic conductivity was investigated by electrochemical impedance spectroscopy (EIS), which is a particularly important parameter to estimate the electrochemical performance of PEs. **Figure 6a** and **Figure S17** show that the ionic conductivity increases with an increase of PEGDA chain length. The ionic conductivity of the PEGDA₆₀₀-S-POSS with a longer PEG crosslinking chain and the controlled networks formed via the thiol-Michael reaction is $5.0 \times 10^{-5} \text{ S cm}^{-1}$ at 30 °C and $2.3 \times 10^{-4} \text{ S cm}^{-1}$ at 60 °C, which is far higher than that of PEGDA₂₀₀-S-POSS. This is because the PEO chain segment motion depends on the ability to undergo conformational changes. The PEGDA₂₀₀-S-POSS with the short PEG chain possesses the rigid cross-linked network, which is not beneficial to conducting the lithium ions effectively. The ionic conductivity results are in accordance with the T_g change shown in DSC curves, which further indicates that the controlled and flexible cross-linked PEG chain contribute to the ion conduction. Besides the polymer chain length, the inclusion of inorganic components in the polymer electrolytes is also an important avenue to influence ionic conductivity. The observed high ionic conductivity and good mechanical strength in the PEGDA₆₀₀-S-POSS could be attributed to the uniform hybrid network structure. For PEs based on PEGDA₆₀₀, PEGDA₆₀₀-S-POSS is the one giving the highest ionic conductivity below 80 °C. At high temperatures (> 80 °C), all PEs arrive the similar conductivity, implying that polymer chains in the PEs have similar dynamics.

The linear sweep voltammetry (LSV) curve of PEGDA₆₀₀-S-POSS, which is sandwiched between Li metal and SS, shows a stabilized current density up to 4.5 V (**Figure 6b**), indicating that the PEGDA₆₀₀-S-POSS PE exhibits a major anodic decomposition potential at 4.5 V vs Li⁺/Li. This performance suggests a possible application of the PEGDA₆₀₀-S-POSS in the working charge-discharge potential window between 2.5-4.2 V because there is no significant decomposition reaction in this voltage range, which is able to satisfy the demand of extensively used LiFePO₄ cathode in lithium ion batteries. In addition, the LSV shows an extremely slight and broad reduction profile in the 0.7-1.4 V range, revealing that a solid electrolyte interface (SEI) layer is formed. From the chart of the AC impedance and DC polarization (**Figure S18**), the Li⁺ transference number (t_{Li^+}) of PEGDA₆₀₀-S-POSS at 60 °C can be calculated as 0.25. In order to explore the lithium electrodeposition in PEs, Li | PEGDA₆₀₀-S-POSS | Li cells were prepared to execute galvanostatic cycling experiments at 60 °C. To evaluate the long-term cycling stability of the LIBs based on the polymer electrolytes fabricated via lithium salt-induced thiol-Michael reaction, the symmetric Li | PEGDA₆₀₀-S-POSS | Li cells were prepared to execute galvanostatic cycling experiments at 60 °C. To simulate the lithium stripping/plating process, we designed a cycling procedure of three-hours for both charge and discharge with a current density of 0.05 mA cm⁻² (**Figure 6c**). The voltage-time curve is flat and stable, no decrease in the voltage and no short circuit were observed with a constant polarization for up to 1270 h, demonstrating the good compatibility between the PE and the lithium metal surface. Besides, the impedance evolution is used to evaluate the

interfacial stability of the polymer electrolytes. **Figure S19** shows the nyquist plot of Li | PEGDA₆₀₀-S-POSS | Li symmetric cell at 60 °C with varying storage time. The diameter of distorted semicircle corresponds to the interfacial resistance (R_i) of PEGDA₆₀₀-S-POSS | Li. R_i decreased as the storage time increased, and stabilized after 7 days, suggesting a good interfacial stability between PEGDA₆₀₀-S-POSS and Li electrodes.⁶⁰ The stable interface is beneficial to reducing the solid-state interface impedance and improving the embedding/de-embedding efficiency of lithium ions on the electrode, and the cycle stability of LIBs can be thus improved.

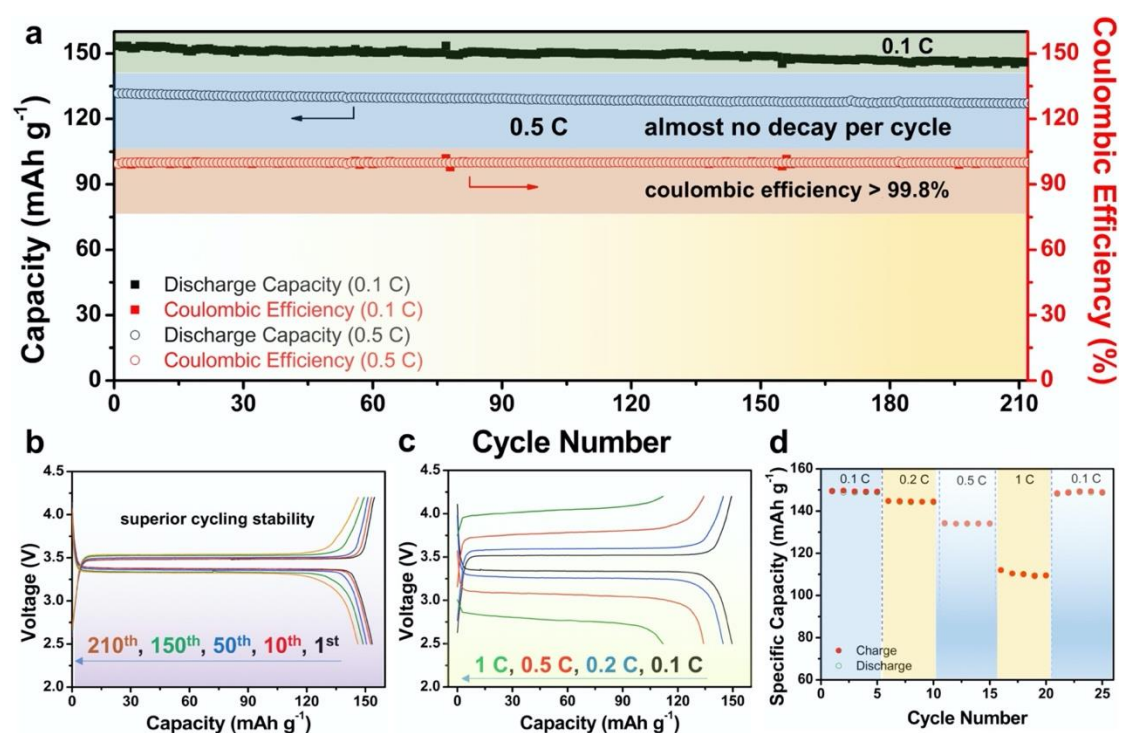


Figure 7. (a) Cycle performance of Li | PEGDA₆₀₀-S-POSS | LFP cell under galvanostatic cycling at 0.1C and 0.5C rates. (b) Charge-discharge curves at 0.1C with PEGDA₆₀₀-S-POSS electrolyte showing low capacity loss and little overpotential. (c) Charge-discharge curves at 0.1C (15 mA g⁻¹), 0.2C (30 mA g⁻¹), 0.5C (75 mA g⁻¹), and 1C (150 mA g⁻¹), which respectively shows a discharge capacity of 149 mAh g⁻¹, 145 mA h g⁻¹, 134 mAh g⁻¹, and 112 mAh g⁻¹. (d) Cycling of Li | PEGDA₆₀₀-S-POSS | LFP battery at 0.1C, 0.2C, 0.5C, and 1C. All experiments were conducted at 60 °C.

To study the potential of the PEGDA₆₀₀-S-POSS PE, LIBs were assembled by combining it with LiFePO₄ (LFP) as cathode and lithium metal as anode. Galvanostatic cycling measurements were conducted under 60 °C at a specific current of 0.1C to explore the cycle performance of the PE in the 2.5-4.2 V voltage range (**Figure 7a**). The PE maintained a specific capacity of 146 mAh g⁻¹ and a coulombic efficiency of 99.8% after 210 cycles. Moreover, the performance of galvanostatic cycling at 0.5C shows little capacity decay and maintains a high coulombic efficiency (99.9%) after 200 cycles. The charge-discharge performance under a constant current (0.1C) at 60 °C is shown in **Figure 7b**. The charge and discharge plateaus are observed at 3.49 V and 3.38 V vs Li⁺/Li, respectively, demonstrating the de-intercalation and intercalation of lithium ion. The charge specific capacity is slightly higher than the discharge specific capacity. However, the difference between charge and discharge plateaus decreases as the charging/discharging process keeps going, illustrating that the reversible reaction contributes to the stabilization of the interface. **Figure 7c** shows the discharge profiles of Li | PEGDA₆₀₀-S-POSS | LFP with charge-discharge current densities over the 0.1-1C range. A discharge capacity of 149 mAh g⁻¹ and a coulombic efficiency of 99.8% are obtained at 0.1C. As the current density increases, the discharge capacity slightly decreased but was nevertheless maintained at relatively high levels (145 mA h g⁻¹ at 0.2C, 134 mAh g⁻¹ at 0.5C, and 112 mAh g⁻¹ at 1C). The lithium battery was tested at different rates to study the durable rate capacity of the PE. The specific capacity at each current density of the Li | PEGDA₆₀₀-S-POSS | LFP battery is depicted in **Figure 7d**. The reversible capacity at 0.2C is 145 mAh g⁻¹, which is comparably high and nearly

equal to the capacity of 0.1C. The reversible capacity at 0.5C and 1C is 134 mAh g⁻¹ and 112 mAh g⁻¹ respectively, which is approximately 90% and 75% of that at 0.1C. More importantly, when the charge-discharge current densities returned to 0.1C, a reversible discharge capacity around 148 mAh g⁻¹ was recovered, demonstrating that the LIBs prepared by using the PEGDA₆₀₀-S-POSS PE have outstanding rate capability.

CONCLUSIONS

As evidenced above, well-defined cross-linked polymer electrolytes based on PEGDA were successfully prepared by a self-catalyzed strategy using base-catalyzed thiol-Michael addition in the presence of lithium (or other alkali metal) salts. In this reaction, the lithium salts act as ion sources and co-catalysts simultaneously. The accelerating action could be correlated with the decrease of electron density in the acrylate vinyl group caused by the interaction between the alkali metal cation and the carbonyl oxygen from acrylate group. This interaction assists the simultaneous delivery of the nucleophilic thiolate anion to the vinyl C_β atom and of a proton from a free thiol to the C_α atom. The different equilibria between the ion pair and the free ions for the salts of different alkali metal cations seems responsible for the stronger accelerating factor exhibited for the salts of the smaller Li cation. The PEs exhibited improved ionic conductivity and thermal stability. Moreover, the Li | PEGDA₆₀₀-S-POSS | LFP cells possessed stable cycling performance. This work paves the way to the development of high-performance polymer batteries via a reliable self-catalyzed strategy.

ASSOCIATED CONTENT

Supporting Information

Scheme S1, Figures S1-S19, and Tables S1-S3

Corresponding Authors

* E-mail zgxue@mail.hust.edu.cn (Z.X.).

* E-mail rinaldo.poli@lcc-toulouse.fr (R.P.).

ORCID

Haiyan Peng: 0000-0002-0083-8589

Xiaolin Xie: 0000-0001-5097-7416

Rinaldo Poli: 0000-0002-5220-2515

Zhigang Xue: 0000-0003-2335-9537

Notes

The authors declare no competing financial interest

ACKNOWLEDGMENT

We are grateful to the National Natural Science Foundation of China (51973073, and 51703080), Natural Science Foundation of Hubei Scientific Committee (2018CFA059), and Applied and Fundamental Frontier Program of Wuhan (2019010701011409) for support of this work. We are also grateful to the CALMIP mesocenter of the University of Toulouse for the allocation of computational resources,

and the Analytical and Testing Center of Huazhong University of Science and Technology for use of measurement facilities.

REFERENCES

- (1) Armand, M.; Tarascon, J.-M., Building Better Batteries. *Nature* **2008**, *451*, 652-657.
- (2) Kang, B.; Ceder, G., Battery Materials for Ultrafast Charging and Discharging. *Nature* **2009**, *458*, 190-193.
- (3) Aricò, A. S.; Bruce, P.; Scrosati, B.; Tarascon, J.-M.; Schalkwijk, W. V., Nanostructured Materials for Advanced Energy Conversion and Storage Devices. *Nat. Mater.* **2005**, *4*, 366-377.
- (4) Winter, M.; Barnett, B.; Xu, K., Before Li Ion Batteries. *Chem. Rev.* **2018**, *118*, 11433-11456.
- (5) Cao, Y.; Li, M.; Lu, J.; Liu, J.; Amine, K., Bridging the Academic and Industrial Metrics for Next-Generation Practical Batteries. *Nat. Nanotechnol.* **2019**, *14*, 200-207.
- (6) Goodenough, J. B.; Park, K. S., The Li-Ion Rechargeable Battery: A Perspective. *J. Am. Chem. Soc.* **2013**, *135*, 1167-76.
- (7) Tarascon, J.-M.; Armand, M., Issues and Challenges Facing Rechargeable Lithium Batteries. *Nature* **2001**, *414*, 369-367.
- (8) Hammami, A.; Raymond, N.; Armand, M., Lithium-Ion Batteries: Runaway Risk of Forming Toxic Compounds. *Nature* **2003**, *424*, 635-636.
- (9) Lopez, J.; Mackanic, D. G.; Cui, Y.; Bao, Z., Designing Polymers for Advanced Battery Chemistries. *Nat. Rev. Mater.* **2019**, *4*, 312-330.
- (10) Zhou, D.; Shanmukaraj, D.; Tkacheva, A.; Armand, M.; Wang, G., Polymer

Electrolytes for Lithium-Based Batteries: Advances and Prospects. *Chem* **2019**, *5*, 2326-2352.

(11) Manthiram, A.; Yu, X. W.; Wang, S. F., Lithium Battery Chemistries Enabled by Solid-State Electrolytes. *Nat. Rev. Mater.* **2017**, *2*, 16103.

(12) Miller, T. F.; Wang, Z.-G.; Coates, G. W.; Balsara, N. P., Designing Polymer Electrolytes for Safe and High Capacity Rechargeable Lithium Batteries. *Acc. Chem. Res.* **2017**, *50*, 590-593.

(13) Xue, Z.; He, D.; Xie, X., Poly(ethylene oxide)-Based Electrolytes for Lithium-Ion Batteries. *J. Mater. Chem. A* **2015**, *3*, 19218-19253.

(14) Xu, H.; Chien, P. H.; Shi, J.; Li, Y.; Wu, N.; Liu, Y.; Hu, Y. Y.; Goodenough, J. B., High-Performance All-Solid-State Batteries Enabled by Salt Bonding to Perovskite in Poly(ethylene oxide). *Proc. Natl. Acad. Sci. USA* **2019**, *116*, 18815-18821.

(15) Croce, F.; Appetecchi, G. B.; Persi, L.; Scrosati, B., Nanocomposite Polymer Electrolytes for Lithium Batteries. *Nature* **1998**, *394*, 456-458.

(16) Zeng, X.-X.; Yin, Y.-X.; Li, N.-W.; Du, W.-C.; Guo, Y.-G.; Wan, L.-J., Reshaping Lithium Plating/Stripping Behavior via Bifunctional Polymer Electrolyte for Room-Temperature Solid Li Metal Batteries. *J. Am. Chem. Soc.* **2016**, *138*, 15825-15828.

(17) Choudhury, S.; Mangal, R.; Agrawal, A.; Archer, L. A., A Highly Reversible Room-Temperature Lithium Metal Battery Based on Crosslinked Hairy Nanoparticles. *Nat. Commun.* **2015**, *6*, 10101.

(18) Choudhury, S.; Stalin, S.; Vu, D.; Warren, A.; Deng, Y.; Biswal, P.; Archer, L. A., Solid-State Polymer Electrolytes for High-Performance Lithium Metal Batteries. *Nat.*

Commun. **2019**, *10*, 4398.

(19) Lu, Q.; He, Y. B.; Yu, Q.; Li, B.; Kaneti, Y. V.; Yao, Y.; Kang, F.; Yang, Q. H., Dendrite-Free, High-Rate, Long-Life Lithium Metal Batteries with A 3D Cross-Linked Network Polymer Electrolyte. *Adv. Mater.* **2017**, *29*, 1604460.

(20) Yu, R.; Li, S.; Chen, G.; Zuo, C.; Zhou, B.; Ni, M.; Peng, H.; Xie, X.; Xue, Z., Monochromatic “Photoinitiator”-Mediated Holographic Photopolymer Electrolytes for Lithium-Ion Batteries. *Adv. Sci.* **2019**, *6*, 1900205 (2019).

(21) Zuo, C.; Yang, M.; Wang, Z.; Jiang, K.; Li, S.; Luo, W.; He, D.; Liu, C.; Xie, X.; Xue, Z., Cyclophosphazene-Based Hybrid Polymer Electrolytes Obtained via Epoxy–Amine Reaction for High-Performance All-Solid-State Lithium-Ion Batteries. *J. Mater. Chem. A* **2019**, *7*, 18871-18879.

(22) Lin, D. C.; Yuen, P. Y.; Liu, Y. Y.; Liu, W.; Liu, N.; Dauskardt, R. H.; Cui, Y., A Silica-Aerogel-Reinforced Composite Polymer Electrolyte with High Ionic Conductivity and High Modulus. *Adv. Mater.* **2018**, *30*, 1802661.

(23) Wan, J.; Xie, J.; Kong, X.; Liu, Z.; Liu, K.; Shi, F.; Pei, A.; Chen, H.; Chen, W.; Chen, J.; Zhang, X.; Zong, L.; Wang, J.; Chen, L. Q.; Qin, J.; Cui, Y., Ultrathin, Flexible, Solid Polymer Composite Electrolyte Enabled with Aligned Nanoporous Host for Lithium Batteries. *Nat. Nanotechnol.* **2019**, *14*, 705-711.

(24) Gao, Y.; Yan, Z.; Gray, J. L.; He, X.; Wang, D.; Chen, T.; Huang, Q.; Li, Y. C.; Wang, H.; Kim, S. H.; Mallouk, T. E.; Wang, D., Polymer–Inorganic Solid–Electrolyte Interphase for Stable Lithium Metal Batteries under Lean Electrolyte Conditions. *Nat. Mater.* **2019**, *18*, 384-389.

- (25) Lin, D.; Liu, W.; Liu, Y.; Lee, H. R.; Hsu, P.-C.; Liu, K.; Cui, Y., High Ionic Conductivity of Composite Solid Polymer Electrolyte via In Situ Synthesis of Monodispersed SiO₂ Nanospheres in Poly(ethylene oxide). *Nano Lett.* **2016**, *16*, 459-465.
- (26) Pan, Q.; Smith, D. M.; Qi, H.; Wang, S.; Li, C. Y., Hybrid Electrolytes with Controlled Network Structures for Lithium Metal Batteries. *Adv. Mater.* **2015**, *27*, 5995-6001.
- (27) Zhou, B.; Jo, Y. H.; Wang, R.; He, D.; Zhou, X.; Xie, X.; Xue, Z., Self-Healing Composite Polymer Electrolyte Formed via Supramolecular Networks for High-Performance Lithium-Ion Batteries. *J. Mater. Chem. A* **2019**, *7*, 10354-10362.
- (28) Hu, J.; Wang, W.; Zhou, B.; Feng, Y.; Xie, X.; Xue, Z., Poly(ethylene oxide)-Based Composite Polymer Electrolytes Embedding with Ionic Bond Modified Nanoparticles for All-Solid-State Lithium-Ion Battery. *J. Membr. Sci.* **2019**, *575*, 200-208.
- (29) Mather, B. D.; Viswanathan, K.; Miller, K. M.; Long, T. E., Michael Addition Reactions in Macromolecular Design for Emerging Technologies. *Prog. Polym. Sci.* **2006**, *31*, 487-531.
- (30) Hoyle, C. E.; Lowe, A. B.; Bowman, C. N., Thiol-Click Chemistry: A Multifaceted Toolbox for Small Molecule and Polymer Synthesis. *Chem. Soc. Rev.* **2010**, *39*, 1355-1387.
- (31) Nair, D. P.; Podgórski, M.; Chatani, S.; Gong, T.; Xi, W.; Fenoli, C. R.; Bowman, C. N., The Thiol-Michael Addition Click Reaction: A Powerful and Widely Used Tool in Materials Chemistry. *Chem. Mater.* **2014**, *26*, 724-744.

- (32) Tasdelen, M. A.; Kiskan, B.; Yagci, Y., Externally Stimulated Click Reactions for Macromolecular Syntheses. *Prog. Polym. Sci.* **2016**, *52*, 19-78.
- (33) Worrell, B. T.; McBride, M. K.; Lyon, G. B.; Cox, L. M.; Wang, C.; Mavila, S.; Lim, C.-H.; Coley, H. M.; Musgrave, C. B.; Ding, Y.; Bowman, C. N., Bistable and Photoswitchable States of Matter. *Nat. Commun.* **2018**, *9*, 2804.
- (34) Chatani, S.; Podgórski, M.; Wang, C.; Bowman, C. N., Facile and Efficient Synthesis of Dendrimers and One-Pot Preparation of Dendritic–Linear Polymer Conjugates via a Single Chemistry: Utilization of Kinetically Selective Thiol–Michael Addition Reactions. *Macromolecules* **2014**, *47*, 4894-4900.
- (35) Hu, J.; Wang, W.; Peng, H.; Guo, M.; Feng, Y.; Xue, Z.; Ye, Y.; Xie, X., Flexible Organic-Inorganic Hybrid Solid Electrolytes Formed via Thiol-Acrylate Photopolymerization. *Macromolecules* **2017**, *50*, 1970-1980.
- (36) Hong, T.; Cao, P.-F.; Zhao, S.; Li, B.; Smith, C.; Lehmann, M.; Erwin, A. J.; Mahurin, S. M.; Venna, S. R.; Sokolov, A. P.; Saito, T., Tailored CO₂-philic Gas Separation Membranes via One-Pot Thiol–ene Chemistry. *Macromolecules* **2019**, *52*, 5819-5828.
- (37) Fang, L.; Sun, J.; Chen, X.; Tao, Y.; Zhou, J.; Wang, C.; Fang, Q., Phosphorus- and Sulfur-Containing High-Refractive-Index Polymers with High T_g and Transparency Derived from a Bio-Based Aldehyde. *Macromolecules* **2020**, *53*, 125-131.
- (38) Grewal, M. S.; Tanaka, M.; Kawakami, H., Bifunctional Poly(ethylene glycol) Based Crosslinked Network Polymers as Electrolytes for All-Solid-State Lithium Ion Batteries. *Polym. Int.* **2019**, *68*, 684-693.

- (39) Suk, J.; Lee, Y. H.; Kim, D. Y.; Kim, D. W.; Cho, S. Y.; Kim, J. M.; Kang, Y., Semi-Interpenetrating Solid Polymer Electrolyte Based on Thiol-Ene Cross-Linker for All-Solid-State Lithium Batteries. *J. Power Sources* **2016**, *334*, 154-161.
- (40) Zhong, Y.; Nguyen, G. T. M.; Plesse, C.; Vidal, F.; Jager, E. W. H., Tailorable, 3D Structured and Micro-Patternable Ionogels for Flexible and Stretchable Electrochemical Devices. *J. Mater. Chem. C* **2019**, *7*, 256-266.
- (41) Xi, W.; Peng, H.; Aguirre-Soto, A.; Kloxin, C. J.; Stansbury, J. W.; Bowman, C. N., Spatial and Temporal Control of Thiol-Michael Addition via Photocaged Superbase in Photopatterning and Two-Stage Polymer Networks Formation. *Macromolecules* **2014**, *47*, 6159-6165.
- (42) Zhang, X.; Xi, W.; Gao, G.; Wang, X.; Stansbury, J. W.; Bowman, C. N., *o*-Nitrobenzyl-Based Photobase Generators: Efficient Photoinitiators for Visible-Light Induced Thiol-Michael Addition Photopolymerization. *ACS Macro Lett.* **2018**, *7*, 852-857.
- (43) Huang, S.; Sinha, J.; Podgórski, M.; Zhang, X.; Claudino, M.; Bowman, C. N., Mechanistic Modeling of the Thiol-Michael Addition Polymerization Kinetics: Structural Effects of the Thiol And Vinyl Monomers. *Macromolecules* **2018**, *51*, 5979-5988.
- (44) Miwa, Y.; Tsutsumi, H.; Oishi, T., Polymerization of Bis-Oxetanes Consisting of Oligo-Ethylene Oxide Chain with Lithium Salts as Initiators. *Polym. J.* **2001**, *33*, 568-574.
- (45) Cui, Y.; Liang, X.; Chai, J.; Cui, Z.; Wang, Q.; He, W.; Liu, X.; Liu, Z.; Cui, G.;

Feng, J., High Performance Solid Polymer Electrolytes for Rechargeable Batteries: A Self-Catalyzed Strategy Toward Facile Synthesis. *Adv. Sci.* **2017**, *4*, 1700174.

(46) Liu, F.-Q.; Wang, W.-P.; Yin, Y.-X.; Zhang, S.-F.; Shi, J.-L.; Wang, L.; Zhang, X.-D.; Zheng, Y.; Zhou, J.-J.; Li, L.; Guo, Y.-G., Upgrading Traditional Liquid Electrolyte via In Situ Gelation for Future Lithium Metal Batteries. *Sci. Adv.* **2018**, *4*, eaat5383.

(47) Zhao, Q.; Liu, X.; Stalin, S.; Khan, K.; Archer, L. A., Solid-State Polymer Electrolytes with In-Built Fast Interfacial Transport for Secondary Lithium Batteries. *Nat. Energy* **2019**, *4*, 365-373.

(48) Dirican, M.; Yan, C.; Zhu, P.; Zhang, X., Composite Solid Electrolytes for All-Solid-State Lithium Batteries. *Mater. Sci. Eng. R: Rep.* **2019**, *136*, 27-46.

(49) Xia, S.; Lopez, J.; Liang, C.; Zhang, Z.; Bao, Z.; Cui, Y.; Liu, W., High-Rate and Large-Capacity Lithium Metal Anode Enabled by Volume Conformal and Self-Healable Composite Polymer Electrolyte. *Adv. Sci.* **2019**, *6*, 1802353.

(50) Zhang, X.; Xie, J.; Shi, F.; Lin, D.; Liu, Y.; Liu, W.; Pei, A.; Gong, Y.; Wang, H.; Liu, K.; Xiang, Y.; Cui, Y., Vertically Aligned and Continuous Nanoscale Ceramic-Polymer Interfaces in Composite Solid Polymer Electrolytes for Enhanced Ionic Conductivity. *Nano Lett.* **2018**, *18*, 3829-3838.

(51) Frisch, M. J.; Trucks, G. W.; Schlegel, H. B.; Scuseria, G. E.; Robb, M. A.; Cheeseman, J. R.; Scalmani, G.; Barone, V.; Mennucci, B.; Petersson, G. A.; Nakatsuji, H.; Caricato, M.; Li, X.; Hratchian, H. P.; Izmaylov, A. F.; Bloino, J.; Zheng, G.; Sonnenberg, J. L.; Hada, M.; Ehara, M.; Toyota, K.; Fukuda, R.; Hasegawa, J.; Ishida, M.; Nakajima, T.; Honda, Y.; Kitao, O.; Nakai, H.; Vreven, T.; Montgomery Jr., J. A.;

Peralta, J. E.; Ogliaro, F.; Bearpark, M.; Heyd, J. J.; Brothers, E.; Kudin, K. N.; Staroverov, V. N.; Kobayashi, R.; Normand, J.; Raghavachari, K.; Rendell, A.; Burant, J. C.; Iyengar, S. S.; Tomasi, J.; Cossi, M.; Rega, N.; Millam, N. J.; Klene, M.; Knox, J. E.; Cross, J. B.; Bakken, V.; Adamo, C.; Jaramillo, J.; Gomperts, R.; Stratmann, R. E.; Yazyev, O.; Austin, A. J.; Cammi, R.; Pomelli, C.; Ochterski, J. W.; Martin, R. L.; Morokuma, K.; Zakrzewski, V. G.; Voth, G. A.; Salvador, P.; Dannenberg, J. J.; Dapprich, S.; Daniels, A. D.; Farkas, Ö.; Foresman, J. B.; Ortiz, J. V.; Cioslowski, J.; Fox, D. J., *Gaussian 09, Revision D.01*. Gaussian, Inc.: Wallingford CT, 2009.

(52) Grimme, S.; Antony, J.; Ehrlich, S.; Krieg, H., A Consistent and Accurate Ab Initio Parametrization of Density Functional Dispersion Correction (DFT-D) for the 94 Elements H-Pu. *J. Chem. Phys.* **2010**, *132*, 154104.

(53) Bryantsev, V. S.; Diallo, M. S.; Goddard III, W. A., Calculation of Solvation Free Energies of Charged Solutes Using Mixed Cluster/Continuum Models *J. Phys. Chem. B* **2008**, *112*, 9709-9719.

(54) Wolinski, K.; Hinton, J. F.; Pulay, P., Efficient Implementation of the Gauge-Independent Atomic Orbital Method for NMR Chemical Shift Calculations. *J. Am. Chem. Soc.* **1990**, *112*, 8251-8260.

(55) Tan, G.; Wu, F.; Zhan, C.; Wang, J.; Mu, D.; Lu, J.; Amine, K., Solid-State Li-Ion Batteries Using Fast, Stable, Glassy Nanocomposite Electrolytes for Good Safety and Long Cycle-Life. *Nano Lett.* **2016**, *16*, 1960-1968.

(56) Duan, H.; Yin, Y.-X.; Zeng, X.-X.; Li, J.-Y.; Shi, J.-L.; Shi, Y.; Wen, R.; Guo, Y.-G.; Wan, L.-J., In-Situ Plasticized Polymer Electrolyte with Double-Network for

- Flexible Solid-State Lithium-Metal Batteries. *Energy Storage Mater.* **2019**, *10*, 85-91.
- (57) Tanaka, Y.; Kuwabara, R.; Na, Y.-H.; Kurokawa, T.; Gong, J.-P.; Osada, Y., Determination of Fracture Energy of High Strength Double Network Hydrogels. *J. Phys. Chem. B* **2005**, *109*, 11559–11562.
- (58) Wu, H.; Cao, Y.; Su, H.; Wang, C., Tough Gel Electrolyte Using Double Polymer Network Design for the Safe, Stable Cycling of Lithium Metal Anode. *Angew. Chem. Int. Ed.* **2018**, *57*, 1361-1365.
- (59) Stoeva, Z.; Martin-Litas, I.; Staunton, E.; Andreev, Y. G.; Bruce, P. G., Ionic Conductivity in the Crystalline Polymer Electrolytes PEO₆:LiXF₆, X = P, As, Sb. *J. Am. Chem. Soc.* **2003**, *125*, 4619-4626.
- (60) Wang, S.; Liu, X.; Wang, A.; Wang, Z.; Chen, J.; Zeng, Q.; Jiang, X.; Zhou, H.; Zhang, L., High-Performance All-Solid-State Polymer Electrolyte with Controllable Conductivity Pathway Formed by Self-Assembly of Reactive Discogen and Immobilized via a Facile Photopolymerization for a Lithium-Ion Battery. *ACS Appl. Mater. Interfaces* **2018**, *10*, 25273–25284.